COMPARISON OF INVERSION METHODS FOR MAIZE CANOPY TIME-SERIES LAI BASED ON SUPREME RECONSTRUCTED IMAGES

Yan Li[1,2], Jin Z. Huang[1], Wan L. Gao[1,3], Jing D. Jia[3], Sha Tao[1,3,*], Yan Z. Ren[4,**], Xin L. Liu[1,4]

[1] College of Information and Electrical Engineering, China Agricultural University, Beijing, China.
[2] College of Urban Construction, Hebei Normal University of Science and Technology, Qinhuangdao, Hebei, China.
[3] Key Laboratory of Agricultural Information Standardization, Ministry of Agriculture and Rural Affairs, Beijing, China.
[4] School of Computer Science and Engineering, Beijing Technology and Business University, Beijing, China.
Correspondence: [*]taosha20070608@163.com, [**]xiaozhaochina@163.com

HIGHLIGHTS

- The Sentinel-2 images are reconstructed by the SupReME algorithm to obtain rich spatial features and consistent spectral reflectance.
- The reconstructed images are more advantageous for LAI estimation than the original images.
- The PROSAIL coupled RF model is verified to be an effective method for time-series LAI estimation at 10 m spatial resolution.

ABSTRACT. *Accurate time-series crop leaf area index (LAI) monitoring can provide data support for field management and early yield estimation. The Sentinel-2 satellite has a high spatial, temporal, and spectral resolution, and its unique three red-edge bands provide an ideal data source for LAI estimation. However, the inconsistent spatial resolution of different bands hinders the application potential of Sentinel-2 images. In view of this problem, we focused on mining more information provided by the high spatial resolution bands of Sentinel-2 images using the Super-Resolution for Multispectral Multiresolution Estimation (SupReME) algorithm. Furthermore, The SNAP (Sentinel Application Platform) biophysical processor and the PROSAIL radiation transfer model coupled with Random Forest (RF) model were applied to estimate time-series LAI of maize canopy at 10 m spatial resolution, and the Leaf Area Index Wireless Sensor Network (LAINet) measurements were used for accuracy verification. Finally, the effectiveness of images reconstructed by SupReME and the two inversion methods for time-series LAI estimation were evaluated. The results showed that: (1) the Sentinel-2 images reconstructed by SupReME can improve spatial characteristics while maintaining spectral invariance, and they were more advantageous for LAI estimation than the original images; (2) The SNAP biophysical processor suits a quick large-scale estimation with robustness, while the PROSAIL coupled RF model achieved a higher coefficient of determination (R^2) and a lower root mean square error (RMSE) (R^2 increased by more than 0.1, RMSE decreased by more than 0.33) for time-series LAI estimation in this specific study area; (3) both inversion methods showed apparent underestimation at the late growth stage. This study verifies the feasibility of obtaining high spatial resolution images using a super-resolution algorithm for LAI inversion and provides the effect of two commonly used inversion methods for time-series LAI estimation at 10 m resolution.*

Keywords. *Leaf area index, PROSAIL model, Random forest, SNAP biophysical processor, SupReME algorithm.*

Leaf area index (LAI), defined as half of the total intercepting area per unit of ground surface area, is closely related to canopy physiological processes (Chen and Black, 1992; Fang et al., 2019). The Global Climate Observing System (GCOS) includes it as one of the vital biophysical parameters among the 18 terrestrial Essential Climate Variables (GCOS, 2016). Since LAI varies with crop growth throughout the entire growing season, consequent and accurate monitoring of the seasonal variation of time-series LAI is critical to yield estimation and agriculture policy development.

Remote sensing satellites with high spatial resolution can provide more abundant and accurate crop canopy information, which is an important data source for precision agricultural development (Sibanda et al., 2015; Xu et al., 2020). The Sentinel-2 satellite incorporates three red-edge bands which are sensitive to vegetation dynamics due to the transition from chlorophyll absorption in the red region to

Submitted for review on 30 December 2021 as manuscript number ITSC 15011; approved for publication as a Research Article by Associate Editor Dr. Chenghai Yang and Community Editor Dr. Naiqian Zhang of the Information Technology, Sensors, & Control Systems Community of ASABE on 27 June 2022.

  ISSN 2769-3295 https://doi.org/10.13031/ja.15011

cellular scattering in NIR (Sibanda et al., 2015; Atzberger and Richter, 2012; Xie et al., 2018; Xing et al., 2020). This makes the Sentinel-2 satellite play a key role in various applications with high spatiotemporal resolutions, especially for vegetation growth monitoring (Pałaś and Zawadzki, 2020; Hu et al., 2020; Djamai et al., 2019b). However, the spatial resolution of Sentinel-2 images varies over its spectral band, including four bands of 10 m resolution, six bands of 20 m resolution, and three bands of 60 m resolution. To fully exploit the image information, various super-resolution reconstruction algorithms that reconstruct the low/medium resolution bands (20 m and 60 m) to a higher resolution (10 m) were proposed (He et al., 2022; Dong et al., 2021). Area-to-Point Regression Kriging (ATPRK) (Wang et al., 2015), a generalized sharpening algorithm proposed by Wang et al., has been verified to successfully sharpen the 20 m resolution bands of the Sentinel-2 image with the 10 m resolution bands (Wang et al., 2016; Wang and Atkinson, 2018). Lanaras et al. (2017) proposed the Super-Resolution for the Multispectral Multiresolution Estimation (SupReME) algorithm and tested it on the reconstruction of simulated and observed Sentinel-2 images with better quality. At present, super-resolution reconstruction algorithms have been developed maturely, but few studies are on the quantitative monitoring of vegetation growth dynamics from super-resolution reconstructed images. Zhang et al. (2019) investigated the feasibility of the SupReME reconstructed images for estimating the canopy LAI and chlorophyll of maize. but only single-period remote sensing images were used in the study. The effect of continuous dynamic monitoring of crop growth based on time-series SupReME reconstructed images still needs further exploration.

The PROSAIL radiative transfer model inverts target parameters by linking the model-simulated crop canopy spectral reflectance with the spectral reflectance from satellite observations and is commonly used in the quantitative inversion of crop growth parameters (Thorp et al., 2012; Zhang et al., 2021; Berger et al., 2018). The SNAP biophysical processor, coupled PROSAIL and inverse artificial neural networks can rapidly calculate biophysical parameters such as LAI from atmospherically corrected Sentinel-2 images (Xie et al., 2019). The applicability of the SNAP biophysical processor to estimate LAI at 20 m spatial resolution has been evaluated in different regions (Djamai et al., 2019a; Pasqualotto et al., 2019). In addition, the PROSAIL coupled Random Forest (RF) model has shown to be a feasible LAI inversion method (Chen et al., 2020). However, both of the methods have rarely been validated for estimating LAI at 10 m spatial resolution. In particular, what is the spatial and spectral fidelity of the reconstructed Sentinel-2 images? Are they effective for time-series LAI inversion at a resolution of 10 m? Which method is more applicable? These questions still need further verification.

Therefore, this study focuses on making full use of the high spatial resolution bands provided by Sentinel-2 images and improving the accuracy of time-series LAI inversion. Comparative analysis is conducted in the following three aspects: (1) to verify the spatial and spectral characteristics of the reconstructed Sentinel-2 images by using the SupReME algorithm comprehensively; (2) to investigate the effectiveness of the reconstructed Sentinel-2 images for time-series LAI estimation at 10 m spatial resolution; (3) to evaluate the applicability of the SNAP biophysical processor and the PROSAIL coupled RF model for LAI estimation in a specific study area.

Study Area and Data

Study Area

The study area, Daman station, is located in the middle reaches of the Heihe River basin in northwestern China (38º50′N, 100º20′E). This region is relatively flat and has an arid continental climate. In recent years, the average elevation and annual temperature are 1556 m and 6°C to 8°C, respectively. It is aridity with little rainfall, and the annual precipitation is about 140 mm. The main crop in the area is maize, which is usually sown at the end of April and harvested in mid-September (Cheng et al., 2014). The location of the research area and the field distribution of the sample plots are shown in figure 1.

Sentinel-2 Images

The Sentinel-2 image contains 13 spectral bands covering visible, red-edge, near-infrared, water vapor, cirrus, and short-wave infrared, with spatial resolutions of 10 m, 20 m, and 60 m (table 1). The Sentinel-2A and Sentinel-2B satellites complement each other to provide a temporal resolution of 5-d. A total of 12 cloud-free Level-1C Sentinel-2 A/B images of the study area during maize growing season were downloaded from the Copernicus Open Access Hub. The imaging dates were day of year (DOY) 166, DOY 181, DOY 186, DOY 191, DOY 196, DOY 206, DOY 211, DOY 216, DOY 221, DOY 226, DOY 246 and DOY 256 in 2019. Atmospheric correction was performed using the Sen2cor plugin in SNAP software, and the boundary of the study area was cut out by the SNAP software.

Field Data Collection

The field measurements were obtained from the "National Tibetan Plateau Scientific Data Center" (http://data.tpdc.ac.cn). The LAI was collected from the Leaf Area Index Wireless Sensor Network (LAINet), which automatically acquired the multi-angle light transmittance of vegetation canopy at 10 min intervals between 06:00 a.m. and 6:30 p.m. at each node, and the daily LAI was calculated by the Beer-Lambert law based on the relationship between LAI and light transmittance. To mitigate weather-induced bias in the daily LAI values, LAINet measurements were smoothed by a 7-d moving window. The processing of LAINet measurements was described in detail by Qu et al. (2013) and Liu et al. (2018). In 2019, there were six 30 m x 30 m maize plots continuously monitored daily from June 1 to September 20, except for missed measurements of plot 6 on August 4. Therefore, the total number of samples corresponding to the Sentinel-2 images was 71 (12 Sentinel-2 image dates × 6 plots − 1).

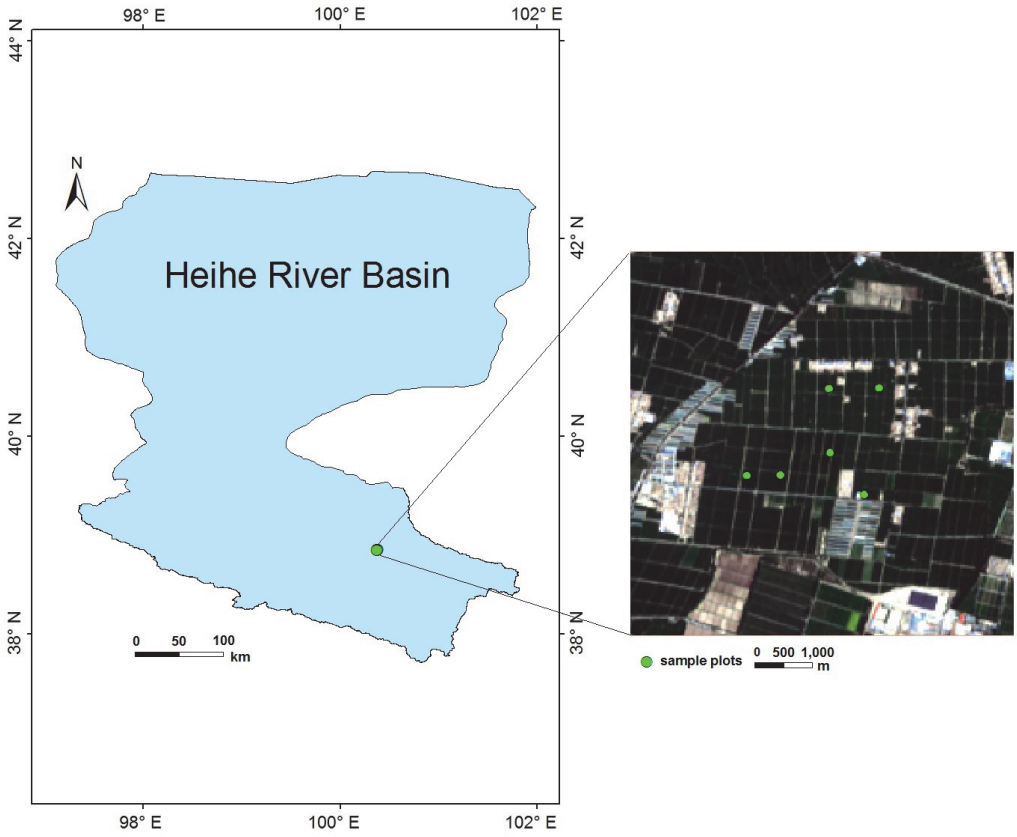

Figure 1. Study site and field sample plots (Basemap: color composite of Sentinel-2 image (R:4 G:3 B:2) on July 30 in 2019).

Table 1. The band information of Sentinel-2 image used in this study.

Bands No.	Spatial resolution (m)	Central wavelength (nm)	Bandwidth (nm)
Band 2 (Blue)	10	490	98
Band 3 (Green)		560	45
Band 4 (Red)		665	38
Band 8 (Near-infrared)		842	145
Band 5 (Red edge 1)	20	705	20
Band 6 (Red edge 2)		740	18
Band 7 (Red edge 3)		783	28
Band 8a (Near-infrared narrow)		865	32
Band 11 (Shortwave infrared 1)		1610	143
Band 12 (Shortwave infrared 2)		2190	238
Band1	60	443	45
Band 9 (Water vapor)		945	26

METHOD

In this study, the Sentinel-2 spectral reflectance of 20 m and 60 m spatial resolution were reconstructed to 10 m using the SupReME algorithm, and LAI was estimated by the SNAP biophysical processor and the PROSAIL coupled RF model based on the reconstructed and original time-series Sentinel-2 images. At each sample location, to alleviate the potential geo-matching errors, the average value of estimated LAI in the 4 × 4 pixel windows of Sentinel-2 images was assessed against the LAINet measurements with metrics of the coefficient of determination (R^2) and the root means square error (RMSE).

SUPREME ALGORITHM

The SupReME algorithm proposed by Lanaras et al. (2017) was employed to super-resolve the lower-resolution channels (20 m and 60 m) of Sentinel-2 images to the highest available resolution (10 m). Using the texture information of the high-resolution bands, the model can generate the highest resolution bands in a single step by performing the super-resolution algorithm for all the lower resolution bands. It has higher computational efficiency and provides better results than other similar algorithms (Sadeh et al., 2021; Zhang et al., 2019).

The inputs of SupReME contain L = 12 reflectance bands, with L_1 = 4 high resolution bands (10 m), L_2 = 6 medium resolution bands (20 m), and L_6 = 2 low resolution bands (60 m). The output totals 12 bands with 10 m spatial resolution. Thus, the upsampling coefficients are $r_1 = 1$, $r_2 = 2$, and $r_6 = 6$, respectively. The image reflectance values are formatted into vector form: $y = (y_1, ..., y_L)$ denotes the values of each band of the input image, $x = [x_1, ..., x_L]$ represents the values of each band of the unknown output image. The input and output images are correlated by the following observation model (including blurring and downsampling):

$$y = M B x \quad (1)$$

where M and B are two block-diagonal matrices, each sub-block of which acts on a spectral band. For the matrix M, each block represents a sampling of x to obtain y. The blur matrix B is a block-circulant- circulant -block matrix, where each block represents a 2D circular convolution.

However, the number of observations in equation (1) is less than the number of unknowns. A dimensionality reduction is used to project the 13 bands of Sentinel-2 into the 6 (p = 6) largest components of the correlation-based eigendecomposition. More than 99% of the signal energy is retained, and the number of unknowns is reduced. Therefore, the columns of output image X live in the subspace spanned by columns of $U \in R^{L \times p}$.

Next, the following steps are used to solve the subspace: (1) upsampling all bands of y to high resolution by bicubic interpolation method, (2) blurring each band to the strongest blur, and (3) performing singular value decomposition on the blurred data.

Finally, the optimal result is obtained by iterative optimization. More information on the SupReME algorithm is detailed in Lanaras et al. (2017), and the MATLAB code is available on GitHub (https://github.com/lanha/SupReME).

SNAP Biophysical Processor

The SNAP biophysical processor module was employed to investigate its applicability for time-series LAI estimation at 10 m spatial resolution.

The module combines the PROSAIL radiative transfer model, which incorporates the leaf optical model (PROSPECT) and the canopy reflectance model (SAIL), and an artificial neural network for the inversion of LAI and other biophysical parameters (Pasqualotto et al., 2019). First, the PROSPECT model is used to obtain vegetation leaf reflectance and transmittance by emulating the upward and downward radiation fluxes from the leaves. Then, the vegetation leaf reflectance together with environmental parameters, such as soil reflectance and solar altitude angle, are input to the SAIL model, and vegetation canopy reflectance data are further obtained. The training database generated by using the radiative transfer model is expected to be able to better simulate the canopy reflectance under most vegetation types and observation conditions on Earth. Based on the pretrained neural network, a pixel-by-pixel biophysical product on Sentinel-2 images can be quickly inverted.

In this study, the canopy reflectance of Band 3, Band 4, Band 5, Band 6, Band 7, Band 8a, Band 11, and Band 12 in Sentinel-2 images, as well as the solar zenith angle θ_s, the observed zenith angle θ_v, and the geometry of the relative azimuth φ at the time of image sensing were input into the module to invert the maize canopy LAI.

PROSAIL Coupled RF Model

To further evaluate the effectiveness of different LAI estimation methods, the PROSAIL model was applied to simulate the reflectance of the maize canopy according to the growth condition in this study area. The model was coupled with the RF regression algorithm to invert the time-series LAI.

The PROSAIL model is widely used in simulating the canopy spectral reflectance of agricultural fields and grasslands (Kimm et al., 2020). There are six leaf parameters required in the leaf model (PROSPECT 5) and eight parameters required in the canopy model (4 SAIL) (table 2). The leaf reflectance and transmittance simulated by PROSPECT are used as inputs for SAIL. Relevant literature has shown that the reflectance in the visible and near-infrared regions was less sensitive to Cm, N, and Cw, but more affected by Cab, LAI, and ALA in this study area (Wang et al., 2019; Qu et al., 2015; Yu et al., 2020). Therefore, Cab, LAI, and ALA were chosen as sensitive parameters for the PROSAIL model. A summary of the input parameters of the PROSAIL model and the range settings in this study is listed in table 2.

Table 2. The input parameters and range settings in the PROSAIL model.

Parameters	Units	Value/ Range	Step	Distribution
leaf structure parameter (N)		1.3		
leaf chlorophyll content (Cab)	μg/cm2	20-90	5	Gaussian
equivalent water thickness (Cw)	(g/cm2)	0.0095		
leaf dry matter content (Cm)	μg/cm2	0.0015		
brown pigments content (Cb*rown*)	μg/cm2	0		
carotenoid content (Car)	μg/cm2	8		
leaf area index (LAI)		0.05-7	0.05	Gaussian
average leaf angle (ALA)	(°)	30-80	5	Gaussian
Diffuse/total radiation (skyl)		0.2		
soil brightness coefficient (ρsoil)		0.5		
hot spot effect (Hspot)		0.2		
Solar zenith angle (SZA)	(°)	from header file		
viewing zenith angle (VZA)	(°)	from header file		
relative azimuth angle (psi)	(°)	from header file		

SZA, VZA, and psi were obtained from the image header file, and the other parameters were determined by prior knowledge and relevant literature (Wang et al., 2019). According to the parameter settings in table 2, a total of 23,100 data were simulated. For LAI inversion in the next step, the simulated reflectance was spectrally resampled with the spectral response function of the Sentinel-2 satellite to make it consistent with the Sentinel-2 bands.

The RF regression algorithm, which has proven to have good performance in estimating crop growth parameters (Han et al., 2020; Srinet et al., 2019; Li et al., 2021), was coupled with the PROSAIL model to invert temporal LAI. RF takes a decision tree as the basic model, and a series of discrepant decision tree models are usually voted or averaged to obtain the final results (Rastgou et al., 2020). Due to the introduction of randomness, RF has strong adaptability to the dataset, good anti-noise performance, and strong fitting ability. It is not easy to fall into over-fitting (Zouggar and Adla, 2019). In this study, the number of decision trees is determined as 500 according to the plot of the decision tree number versus error, and the number of randomly selected variables M is 1.

Studies have shown that the 2-bands Enhanced Vegetation index (EVI2), Red-edge Chlorophyll index (CIred-edge1), and Green Chlorophyll index (CIgreen) can estimate LAI well (Yu et al., 2020; Sun et al., 2020). Therefore, the

Table 3. The vegetation indices used in the PROSAIL coupled RF model.

Vegetation index	Formula	Reference
EVI2	EV12 = 2.5(NIR−R)/(NIR+2.4R+1)	Jiang et al., 2008
CIgreen	CIgreen=NIR/G-1	Gitelson et al., 2003
CIred-edge1	CIred-edge 1=NIR/Red-edge 1	Gitelson et al., 2003

lookup tables between the above three vegetation indices (table 3) generated by PTOSAIL and LAI were used as training datasets for the inversion model. The corresponding vegetation indices calculated from two sources of Sentinel-2 observations at 10 m spatial resolution were respectively used as test datasets to estimate the time-series LAI of maize canopy. One was resampled by the nearest neighbor method, and the other was reconstructed by SupReME.

Results and Analysis

Characteristic Analysis of Reconstructed Images by SupReME

To explore the performance of the SupReME algorithm in mining image spatial feature, the image on DOY 211 was taken as an example to compare the reconstructed image with the original Sentinel-2 image, as shown in figure 2. It can be seen that the contours of the features on the reconstructed image were consistent with those on the original Sentinel-2 image. This indicated that SupReME performed well in spatial fidelity. Moreover, the reconstructed images were clearer and reflected richer spatial texture features, indicating that SupReME can mine more detailed spatial features of the image.

Table 4. Accuracy analysis of reconstructed image and original image.

Band	Regression equation	AD	RMSE	EDGE	LBP
Band 1	y=1.0375x+0.0001	0.001	0.015	-0.251	0.389
Band 5	y=1.0233x-0.0023	0.000	0.016	0.049	0.002
Band 6	y=1.0352x+0.0134	-0.003	0.017	0.079	0.028
Band 7	y=1.0207x-0.008	0.000	0.018	0.040	-0.009
Band 8a	y=1.0196x-0.0071	0.000	0.018	0.050	-0.009
Band 9	y=1.0475x-0.0174	0.001	0.033	-0.186	0.421
Band 11	y=1.1021x-0.0193	0.000	0.020	0.062	0.086
Band 12	y=1.0545x-0.0068	0.000	0.020	0.090	0.037

To further evaluate the spectral consistency between the reconstructed image and the original Sentinel-2 image quantitatively, the reconstructed bands with 10 m spatial resolution were aggregated to 20 m or 60 m to compare with the original bands of 20 m and 60 m (Band 1, Band 5 to Band 7, Band 8a, Band 9, Band 11 and Band 12). A novel assess framework with four accuracy metrics, including RMSE, average difference (AD), Robert's edge (EDGE), and local binary pattern (LBP), was introduced to quantify the spectral and spatial quality in the reconstructed images comprehensively and with less information redundancy (Zhu et al., 2022). AD and RMSE assess the spectral accuracy, and EDGE and LBP assess the spatial accuracy. The closer the values of these metrics are to 0, the better the spectral and spatial fidelity. Table 4 showed the analysis results between the reconstructed image and the original Sentinel-2 image for each band. It can be seen that the spectral reflectance of the images before and after reconstruction was very similar with low values of AD and RMSE, and the maximum value of RMSE was 0.033 (Band 9). From the spatial assess metrics of EDGE and LBP, it can be seen that the spatial texture features of Band 1 and Band 9 with 60m resolution in original images produced a slightly larger error than other bands, which all maintained values below 0.1. Therefore, the

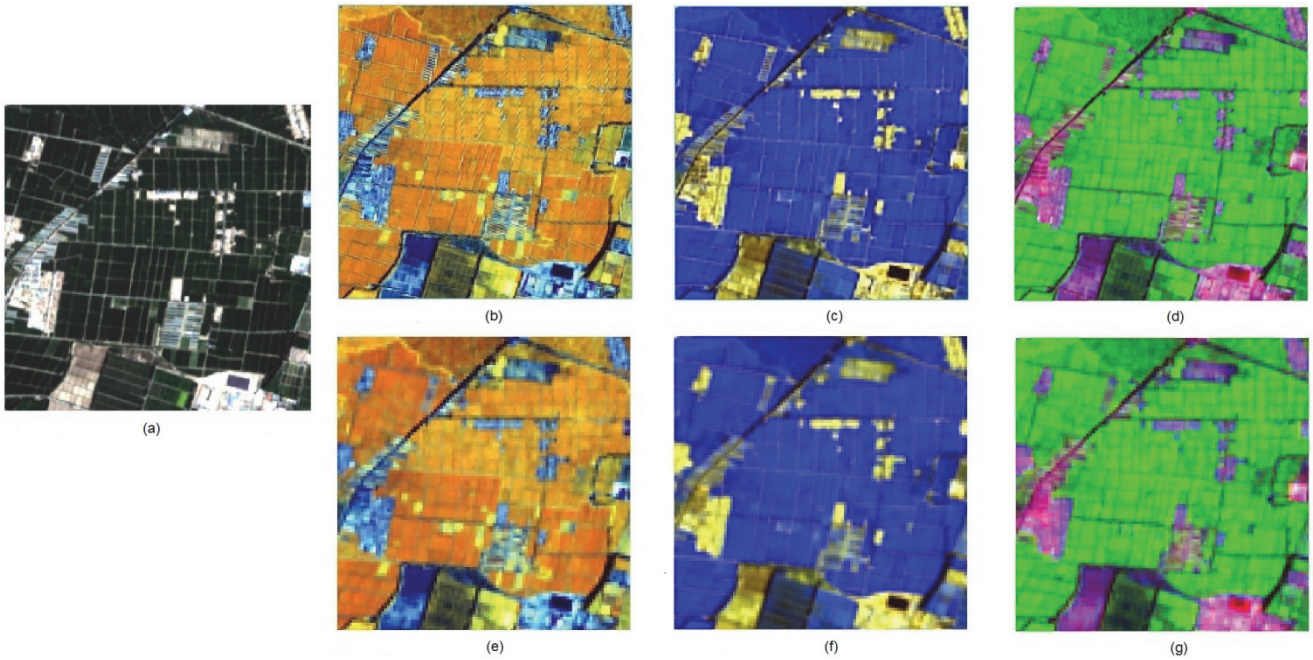

Figure 2. Image reconstructed results using SupReME algorithm: (a) original 10 m true color composite (R:4 G:3 B:2), (b) reconstructed 10 m false color composite (R:7 G:6 B:5), (c) reconstructed 10 m false color composite (R:12 G:11 B:8a), (d) reconstructed 10 m false color composite (R:1 G:9 B:12), (e) original 20 m false color composite (R:7 G:6 B:5), (f) original 20 m false color composite (R:12 G:11 B:8a), (g) original 20 m false color composite (R:1 G:9 B:12).

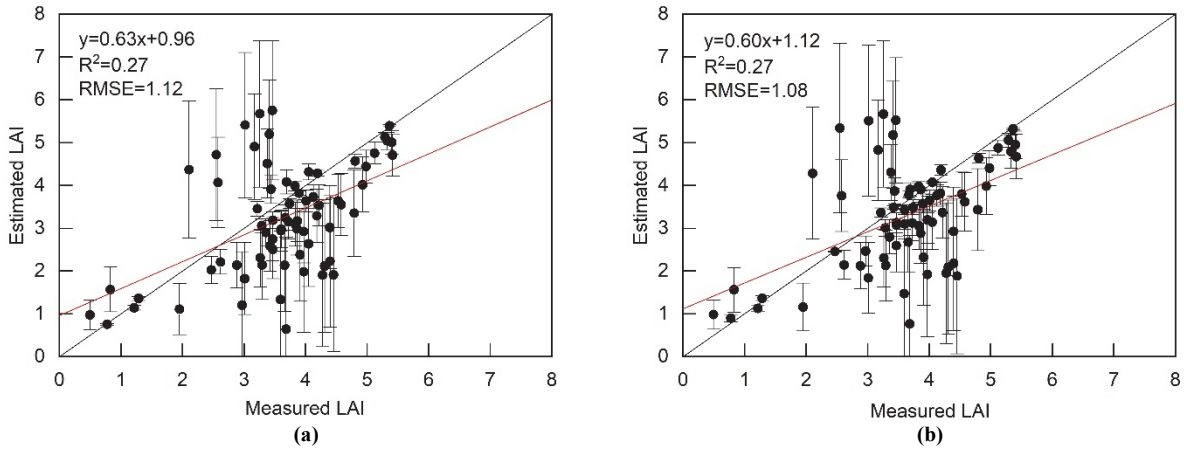

Figure 3. Accuracy comparison of LAI estimated by SNAP biophysical processor: (a) original images and (b) reconstructed images.

images reconstructed by SupReME showed good spectral and spatial consistency with actual observations.

LAI Estimations of SNAP Biophysical Processor

The SNAP biophysical processor has been proven to provide better estimates of crop biophysical parameters at 20 m spatial resolution for Sentinel-2 images, while few studies are about biophysical parameter estimations at 10 m resolution. In this research, LAI at 10 m resolution in Heihe River Basin was generated by the SNAP biophysical processor, and its consistency with LAINet measurements was evaluated. The results were shown in figure 3. There was little difference between LAI estimates from the original and the SupReME reconstructed images. The R^2 values between the LAI estimates and LAINet measurements were both below 0.3, and the RMSE exceeded 1.0. Compared with the original images, the dispersion of LAI estimated by the SNAP biophysical processor from the SupReME reconstructed images was generally smaller. Therefore, it achieved a lower RMSE. However, there were some outliers that produced larger errors, so the linear fit of LAI from the reconstructed images was not as good as that from the original images.

LAI Estimations of PROSAIL Coupled with RF Model

To further evaluate the accuracy of the PROSAIL coupled RF model for time-series LAI estimation at 10 m resolution, the look-up tables between three vegetation indices of EVI2, CIgreen, and CIred-edge1, and LAI were used as the training dataset of the RF model in turn. The original and reconstructed Sentinel-2 images were used as the test datasets. The R^2 and RMSE between the estimated LAI with different vegetation indices and LAINet measurements were compared (table 5). We found that the estimation results from the reconstructed images were better than those from the original images, and both showed the best results based on the model constructed by CIgreen.

Furthermore, the LAI estimated from the original images and the reconstructed images based on the model constructed by CIgreen were compared (fig. 4). It was clear that RMSE was lower than 0.8 for both sources of images, and the estimation results from the reconstructed images (R^2 = 0.42, RMSE = 0.74) were better than those from the original images (R^2 = 0.39, RMSE = 0.78) with less dispersion. This indicated that the reconstructed images were more advantageous for LAI estimation. In addition, the LAI estimated by the PROSAIL coupled RF model was closer to the LAINet measurements than that estimated by the SNAP biophysical processor, with more clustered point distribution. It achieved an improvement of more than 0.1 in R^2 and a reduction of more than 0.3 in RMSE (fig. 3 and fig. 4). But when LAI was larger than 3.5, both methods gave an underestimation. The PROSAIL coupled RF model provided more accurate estimates for most points between 3.5 and 5. However, when LAI was larger than 5, the SNAP biophysical processor produced better results than the PROSAIL coupled RF model. Hence, the linear fit of LAI estimated by the PROSAIL coupled RF model was slightly worse than that of the SNAP biophysical processor.

Table 5. Accuracy comparison of LAI estimated by PROSAIL coupled RF model based on different vegetation indices.

Vegetation index	Original images		Reconstructed images	
	R^2	RMSE	R^2	RMSE
EVI2	0.29	0.80	0.30	0.80
CIgreen	0.39	0.78	0.42	0.74
CIred-edge1	0.29	0.98	0.30	0.97

Analysis of LAI Seasonal Dynamics

To further observe the seasonal dynamics of LAI and to evaluate the estimation accuracy of the SNAP biophysical processor and PROSAIL coupled RF model, based on the reconstructed images, the temporal variation of LAI of the six plots in the study area estimated by the two methods were compared with the LAINet measurements, as shown in figure 5. Both inversion methods can describe the temporal dynamic characteristics of LAI with slight differences in estimates, but there was an underestimation in all plots with the exception of plot 6, especially at the reproductive stage of maize growth (after DOY 212). After DOY 240, the LAINet measurements showed no obvious downward trend, while the remote sensing estimations decreased significantly. Especially large deviations occurred between SNAP estimates and LAINet measurements. For plot 6, the estimates of both methods showed large deviations from the LAINet measurements.

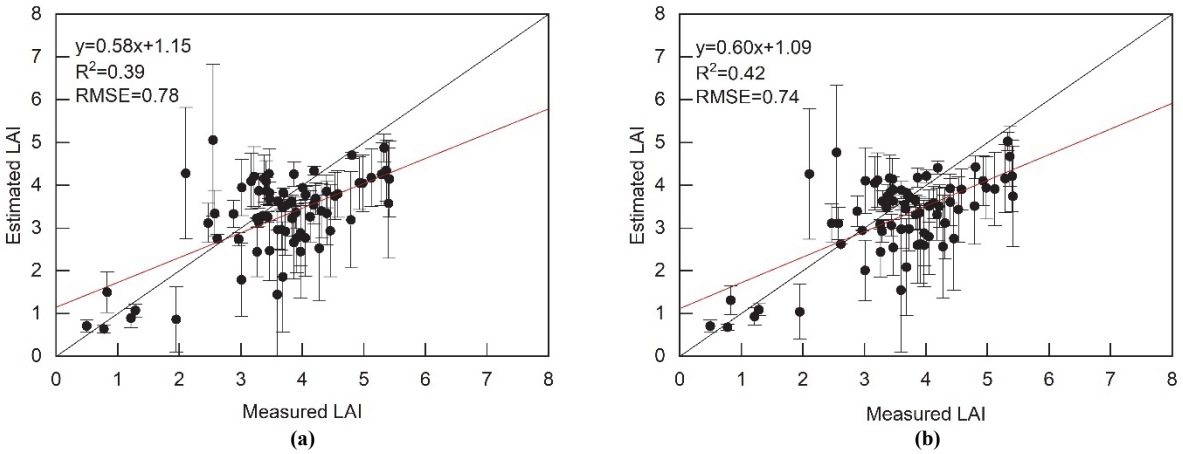

Figure 4. Accuracy comparison of LAI estimated by PROSAIL coupled RF model: (a) original images and (b) reconstructed images.

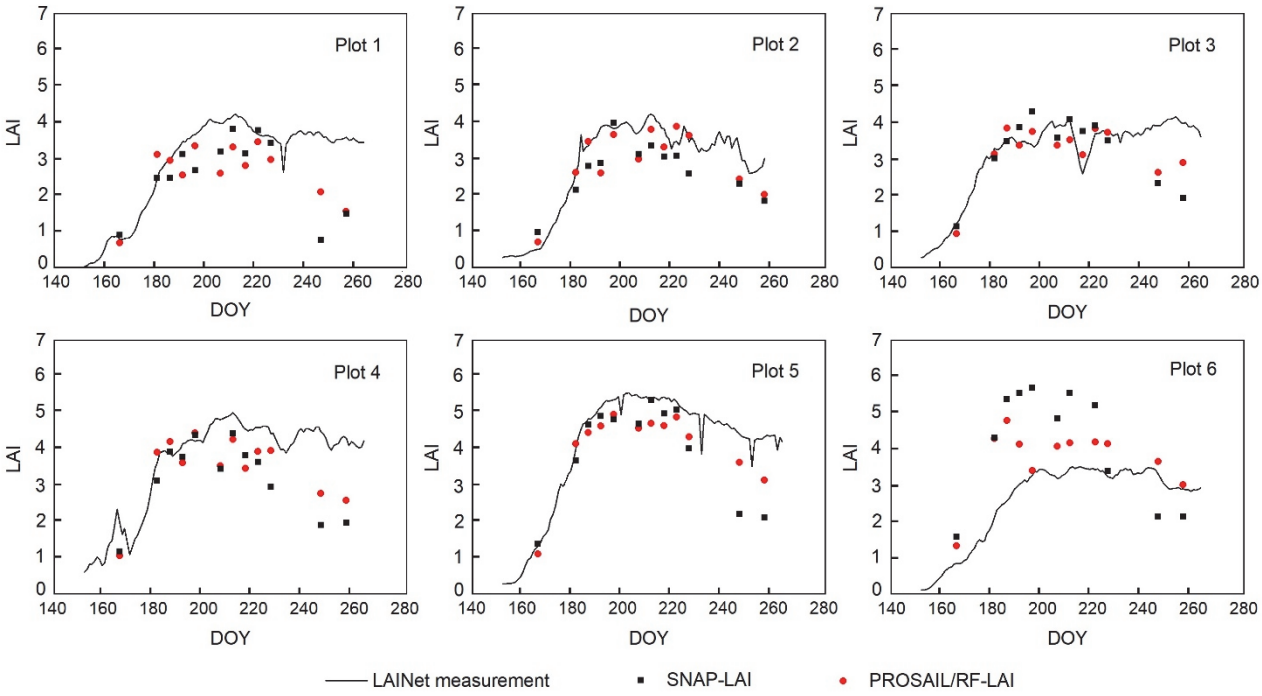

Figure 5. Analysis of time-series LAI of each plot (SNAP-LAI and PROSAIL/RF-LAI represent estimation results of SNAP biophysical processor and PROSAIL coupled RF model, respectively).

DISCUSSION

In order to obtain high spatial resolution remote sensing images, we employ the SupReME algorithm to reconstruct Sentinel-2 images and verify the quality of the reconstructed images from spectral and spatial aspects. The SupReME algorithm reconstructs the coarser-resolution bands of 20 m and 60 m into 10 m with the help of the high-resolution bands in Sentinel-2 images. All bands are from the same sensor with uniform imaging time, imaging geometry conditions, and spectral response, which reduces the uncertainty in the reconstruction process. Therefore, better spatial details and consistent spectrum can be provided, which has also been demonstrated in previous studies (Zhang et al., 2019). Band 1 and Band 9 produce slightly larger errors, but they are not used for subsequent inversions. Therefore, we consider that the SupReME reconstructed images can be used for LAI inversion.

Then, comparative studies are implemented in this research: two data sources of original and SupReME reconstructed images, and two estimation methods of SNAP biophysical processor and PROSAIL coupled RF model. When comparing the two image data sources, the SupReME reconstructed images produce a smaller RMSE, indicating that the finer spatial resolution of the reconstructed images contributes to LAI inversion. The LAI estimated using the SNAP biophysical processor from the two data sources show slight differences, which is probably because it is trained based on global vegetation types and has better robustness. Comparing the two estimation methods, the PROSAIL coupled RF model achieves higher R^2 and lower RMSE, perhaps because the PROSAIL coupled RF model is trained with the simulated maize canopy reflectance just in this study area. The

model input parameters are designed more specifically. However, at the late stage of crop growth, the seasonal dynamic trends of LAI are underestimated by both methods compared to LAINet measurements. On the one hand, spectral saturation is a potential factor causing the discrepancy. On the other hand, LAINet seems to be closer to true LAI than LAI-2000 for maize (Qu et al. 2013), while remote sensing derives the effective LAI.

When LAI is larger than 5, which only appears in plot 5, the SNAP biophysical processor estimates are closer to the LAINet measurements, making it a better linear fit. However, previous research (Yu et al., 2020) has shown that the LAINet measurements of plot 5 are higher than those of the LI-3000 and LAI-2200C, thus we cannot conclude that the SNAP biophysical processor performs better than the PROSAIL coupled RF model. Moreover, it is found that the estimations of plot 6 deviate significantly from the LAINet measurements and the seasonal dynamics of LAI also shows that the LAINet measurements of plot 6 are lower compared with the other plots (fig. 5). Regarding the relevant literature (Yu et al., 2020), the LAI of plot 6 are underestimated by LAINet, which is consistent with the results of this research. Therefore, LAINet has the advantage of automatic and continuous acquisition of field LAI, which significantly reduces manpower. However, the systematic error of LAINet affects the estimation accuracy evaluation to a certain extent, and more validation experiments should be explored in the future.

In addition, it is internationally recognized that high spatial resolution mapping of crop phenological changes needs to be within subweekly temporal frequencies (Malenovský et al., 2012; Li et al., 2022). Although Sentinel-2A and Sentinel-2B images provide a temporal resolution of 5-d when viewed together, it is usually challenging to obtain intensive time-series images due to various unfavorable weather conditions. For example, there is only one image (DOY 246) available during DOY 226 to DOY 256 in this study area, which does not meet the continuous dynamic monitoring requirements of LAI. Therefore, the generation of high spatial resolution and intensive temporal resolution images by combining super-resolution reconstruction algorithm and spatiotemporal fusion method will be focused on in the next step.

Conclusion

The SupReME algorithm was used to reconstruct the coarser-resolution bands of Sentinel-2 image during the maize growing season to a spatial resolution of 10 m. Two inversion methods of the SNAP biophysical processor and the PROSAIL coupled RF model were applied for the original and reconstructed images to estimate time-series LAI. The spatial and spectral characteristics of the reconstructed image and the applicability of the two inversion methods were evaluated. The results of this research show the following conclusions:

- The images reconstructed by the SupReME algorithm can provide rich spatial texture features and well maintain the spectral reflectance.
- The LAI estimation accuracy of both the two inversion methods based on the reconstructed images is higher than that of the original images.
- The SNAP biophysical processor suits a quick large-scale LAI estimation with robustness, while the PROSAIL coupled RF model improves the estimation accuracy with R^2 increased by more than 0.1 and RMSE decreased by more than 0.3. Therefore, the PROSAIL coupled RF model is more recommended than the SNAP biophysical processor for time-series LAI inversion for a specific study area.
- Both the inversion methods can monitor the temporal dynamics of LAI, but the underestimation at the late growth stage is obvious.

Acknowledgments

This work was supported by the Natural Science Foundation of the Hebei Province of China (D2022407001), National Natural Science Foundation of China (31801669), and Open Project Program of the National Engineering Laboratory for Agriproduct Quality Traceability (BTBU, No. AQT-2019-YB10). Thanks to the National Tibetan Plateau Data for providing LAINet measurements. The authors would also like to thank Charis Lanaras for providing SupReME codes.

References

Atzberger, C., & Richter, K. (2012). Spatially constrained inversion of radiative transfer models for improved LAI mapping from future Sentinel-2 imagery. *Remote Sens. Environ., 120*, 208-218. https://doi.org/10.1016/j.rse.2011.10.035

Berger, K., Atzberger, C., Danner, M., D'Urso, G., Mauser, W., Vuolo, F., & Hank, T. (2018). Evaluation of the PROSAIL model capabilities for future hyperspectral model environments: A review study. *Remote Sens., 10*(1), 85. https://doi.org/10.3390/rs10010085

Chen, J. M., & Black, T. A. (1992). Defining leaf area index for non-flat leaves. *Plant Cell Environ., 15*(4), 421-429. https://doi.org/10.1111/j.1365-3040.1992.tb00992.x

Chen, Z., Jia, K., Xiao, C., Wei, D., Zhao, X., Lan, J.,... Wang, L. (2020). Leaf area index estimation algorithm for GF-5 hyperspectral data based on different feature selection and machine learning methods. *Remote Sens., 12*(13), 2110. https://doi.org/10.3390/rs12132110

Cheng, G., Li, X., Zhao, W., Xu, Z., Feng, Q., Xiao, S., & Xiao, H. (2014). Integrated study of the water–ecosystem–economy in the Heihe River Basin. *Natl. Sci. Rev., 1*(3), 413-428. https://doi.org/10.1093/nsr/nwu017

Djamai, N., Fernandes, R., Weiss, M., McNairn, H., & Goïta, K. (2019a). Validation of the sentinel simplified level 2 product prototype processor (SL2P) for mapping cropland biophysical variables using Sentinel-2/MSI and Landsat-8/OLI data. *Remote Sens. Environ., 225*, 416-430. https://doi.org/10.1016/j.rse.2019.03.020

Djamai, N., Zhong, D., Fernandes, R., & Zhou, F. (2019b). Evaluation of vegetation biophysical variables time series derived from synthetic Sentinel-2 images. *Remote Sensing, 11*(13), 1547. https://doi.org/10.3390/rs11131547

Dong, R., Zhang, L., & Fu, H. (2021). RRSGAN: Reference-based super-resolution for remote sensing image. *IEEE Trans. Geosci. Remote Sens., 60*, 1-17. https://doi.org/10.1109/TGRS.2020.3046045

Fang, H., Baret, F., Plummer, S., & Schaepman-Strub, G. (2019). An overview of global leaf area index (LAI): Methods, products, validation, and applications. *Rev. Geophys., 57*(3), 739-799. https://doi.org/10.1029/2018RG000608

GCOS. (2016). The global observing system for climate: Implementation needs (GCOS-200). Geneva, Switzerland: WMOP.

Gitelson, A. A., Gritz, Y., & Merzlyak, M. N. (2003). Relationships between leaf chlorophyll content and spectral reflectance and algorithms for non-destructive chlorophyll assessment in higher plant leaves. *J. Plant Physiol., 160*(3), 271-282. https://doi.org/10.1078/0176-1617-00887

Han, J., Zhang, Z., Cao, J., Luo, Y., Zhang, L., Li, Z., & Zhang, J. (2020). Prediction of winter wheat yield based on multi-source data and machine learning in china. *Remote Sens., 12*(2), 236. https://doi.org/10.3390/rs12020236

He, J., Yuan, Q., Li, J., & Zhang, L. (2022). PoNet: A universal physical optimization-based spectral super-resolution network for arbitrary multispectral images. *Information Fusion, 80*, 205-225. https://doi.org/10.1016/j.inffus.2021.10.016

Hu, Q., Yang, J., Xu, B., Huang, J., Memon, M. S., Yin, G.,... Liu, K. (2020). Evaluation of global decametric-resolution LAI, FAPAR and FVC estimates derived from Sentinel-2 imagery. *Remote Sens., 12*(6), 912.

Jiang, Z., Huete, A. R., Didan, K., & Miura, T. (2008). Development of a two-band enhanced vegetation index without a blue band. *Remote Sens. Environ., 112*(10), 3833-3845. https://doi.org/10.1016/j.rse.2008.06.006

Kimm, H., Guan, K., Jiang, C., Peng, B., Gentry, L. F., Wilkin, S. C.,... Luo, Y. (2020). Deriving high-spatiotemporal-resolution leaf area index for agroecosystems in the U.S. Corn Belt using Planet Labs CubeSat and STAIR fusion data. *Remote Sens. Environ., 239*, 111615. https://doi.org/10.1016/j.rse.2019.111615

Lanaras, C., Bioucas-Dias, J., Baltsavias, E., & Schindler, K. (2017). Super-resolution of multispectral multiresolution images from a single sensor. *Proc. 2017 IEEE Conference on Computer Vision and Pattern Recognition Workshops (CVPRW).* https://doi.org/10.1109/CVPRW.2017.194

Li, Y., Ren, Y. Z., Gao, W. L., Tao, S., Jia, J. D., & Liu, X. L. (2021). Analysis of influencing factors on winter wheat yield estimations based on a multisource remote sensing data fusion. *Appl. Eng. Agric., 37*(5), 991-1003. https://doi.org/10.13031/aea.14398

Li, Y., Ren, Y., Gao, W., Jia, J., Tao, S., & Liu, X. (2022). An enhanced spatiotemporal fusion method – Implications for DNN based time-series LAI estimation by using Sentinel-2 and MODIS. *Field Crops Research, 279*, 108452. https://doi.org/10.1016/j.fcr.2022.108452

Liu, S., Li, X., Xu, Z., Che, T., Xiao, Q., Ma, M.,... Ren, Z. (2018). The heihe integrated observatory network: A basin-scale land surface processes observatory in China. *Vadose Zone J., 17*(1), 180072. https://doi.org/10.2136/vzj2018.04.0072

Malenovský, Z., Rott, H., Cihlar, J., Schaepman, M. E., García-Santos, G., Fernandes, R., & Berger, M. (2012). Sentinels for science: Potential of Sentinel-1, -2, and -3 missions for scientific observations of ocean, cryosphere, and land. *Remote Sens. Environ., 120*, 91-101. https://doi.org/10.1016/j.rse.2011.09.026

Pałaś, K. W., & Zawadzki, J. (2020). Sentinel-2 imagery processing for tree logging observations on the Białowieża forest world heritage site. *Forests, 11*(8), 857. https://doi.org/10.3390/f11080857

Pasqualotto, N., D'Urso, G., Bolognesi, S. F., Belfiore, O. R., Van Wittenberghe, S., Delegido, J.,... Moreno, J. (2019). Retrieval of evapotranspiration from Sentinel-2: Comparison of vegetation indices, semi-empirical models and SNAP biophysical processor approach. *Agron., 9*(10), 663. https://doi.org/10.3390/agronomy9100663

Qu, Y., Han, W., & Ma, M. (2015). Retrieval of a temporal high-resolution Leaf Area Index (LAI) by combining MODIS LAI and ASTER reflectance data. *Remote Sens., 7*(1), 195-210. https://doi.org/10.3390/rs70100195

Qu, Y., Zhu, Y., Han, W., Wang, J., & Ma, M. (2013). Crop leaf area index observations with a wireless sensor network and its potential for validating remote sensing products. *IEEE J-STARS, 7*(2), 431-444. https://doi.org/10.1109/JSTARS.2013.2289931

Rastgou, M., Bayat, H., Mansoorizadeh, M., & Gregory, A. S. (2020). Estimating the soil water retention curve: Comparison of multiple nonlinear regression approach and random forest data mining technique. *Comput. Electron. Agric., 174*, 105502. https://doi.org/10.1016/j.compag.2020.105502

Sadeh, Y., Zhu, X., Dunkerley, D., Walker, J. P., Zhang, Y., Rozenstein, O.,... Chenu, K. (2021). Fusion of Sentinel-2 and PlanetScope time-series data into daily 3 m surface reflectance and wheat LAI monitoring. *Int. J. Appl. Earth Obs. Geoinf., 96*, 102260. https://doi.org/10.1016/j.jag.2020.102260

Sibanda, M., Mutanga, O., & Rouget, M. (2015). Examining the potential of Sentinel-2 MSI spectral resolution in quantifying above ground biomass across different fertilizer treatments. *ISPRS J. Photogramm. Remote Sens., 110*, 55-65. https://doi.org/10.1016/j.isprsjprs.2015.10.005

Srinet, R., Nandy, S., & Patel, N. R. (2019). Estimating leaf area index and light extinction coefficient using Random Forest regression algorithm in a tropical moist deciduous forest, India. *Ecol. Inf., 52*, 94-102. https://doi.org/10.1016/j.ecoinf.2019.05.008

Sun, Y., Qin, Q., Ren, H., Zhang, T., & Chen,.. S. (2020). Red-edge band vegetation indices for leaf area index estimation from Sentinel-2/MSI imagery. *IEEE Trans. Geosci. Remote Sens., 58*(2), 826-840. https://doi.org/10.1109/TGRS.2019.2940826

Thorp, K. R., Wang, G., West, A. L., Moran, M. S., Bronson, K. F., White, J. W., & Mon, J. (2012). Estimating crop biophysical properties from remote sensing data by inverting linked radiative transfer and ecophysiological models. *Remote Sens. Environ., 124*, 224-233. https://doi.org/10.1016/j.rse.2012.05.013

Wang, Q., & Atkinson, P. M. (2018). Spatio-temporal fusion for daily Sentinel-2 images. *Remote Sens. Environ., 204*, 31-42. https://doi.org/10.1016/j.rse.2017.10.046

Wang, Q., Shi, W., Atkinson, P. M., & Zhao, Y. (2015). Downscaling MODIS images with area-to-point regression kriging. *Remote Sens. Environ., 166*, 191-204. https://doi.org/10.1016/j.rse.2015.06.003

Wang, Q., Shi, W., Li, Z., & Atkinson, P. M. (2016). Fusion of Sentinel-2 images. *Remote Sens. Environ., 187*, 241-252. https://doi.org/10.1016/j.rse.2016.10.030

Wang, T., Qu, Y., Xia, Z., Peng, Y., & Liu, Z. (2019). Multi-Scale validation of MODIS LAI products based on crop growth period. *ISPRS Int. J. Geo-Inf., 8*(12), 547. https://doi.org/10.3390/ijgi8120547

Xie, Q., Dash, J., Huang, W., Peng, D., Qin, Q., Mortimer., H.,... Ye, H. (2018). Vegetation indices combining the red and red-edge spectral information for leaf area index retrieval. *IEEE J-STARS, 11*(5), 1482-1493. https://doi.org/10.1109/JSTARS.2018.2813281

Xie, Q., Dash, J., Huete, A., Jiang, A., Yin, G., Ding, Y.,... Huang, W. (2019). Retrieval of crop biophysical parameters from Sentinel-2 remote sensing imagery. *Int. J. Appl. Earth Obs. Geoinf., 80*, 187-195. https://doi.org/10.1016/j.jag.2019.04.019

Xing, N., Huang, W., Xie, Q., Shi, Y., Ye, H., Dong, Y.,... Jiao, Q. (2020). A transformed triangular vegetation index for estimating winter wheat leaf area index. *Remote Sens., 12*(1), 16.

Xu, C., Qu, J. J., Hao, X., Cosh, M. H., Zhu, Z., & Gutenberg, L. (2020). Monitoring crop water content for corn and soybean fields through data fusion of MODIS and Landsat measurements in Iowa. *Agric. Water Manage., 227*, 105844. https://doi.org/10.1016/j.agwat.2019.105844

Yu, L., Shang, J., Cheng, Z., Gao, Z., Wang, Z., Tian, L.,... Qu, Y. (2020). Assessment of cornfield LAI Retrieved from multi-source satellite data using continuous field LAI measurements based on a wireless sensor network. *Remote Sens., 12*(20), 3304. https://doi.org/10.3390/rs12203304

Zhang, M., Su, W., Fu, Y., Zhu, D., Xue, J.-H., Huang, J.,... Yao, C. (2019). Super-resolution enhancement of Sentinel-2 image for retrieving LAI and chlorophyll content of summer corn. *Eur. J. Agron., 111*, 125938. https://doi.org/10.1016/j.eja.2019.125938

Zhang, Y., Hui, J., Qin, Q., Sun, Y., Zhang, T., Sun, H., & Li, M. (2021). Transfer-learning-based approach for leaf chlorophyll content estimation of winter wheat from hyperspectral data. *Remote Sens. Environ., 267*, 112724. https://doi.org/10.1016/j.rse.2021.112724

Zhu, X., Zhan, W., Zhou, J., Chen, X., Liang, Z., Xu, S., & Chen, J. (2022). A novel framework to assess all-round performances of spatiotemporal fusion models. *Remote Sens. Environ., 274*, 113002. https://doi.org/10.1016/j.rse.2022.113002

Zouggar, T., & Adla, A. (2019). A diversity-accuracy measure for homogenous ensemble selection. *Int. J. Interact. Multi., 5*. https://doi.org/10.9781/ijimai.2018.06.005